

The Myth of URANS

Daniel M. Israel

ARTICLE HISTORY

Compiled December 5, 2022

Abstract

Since the 1990s, RANS practitioners have observed spontaneous unsteadiness in RANS simulations. Some have suggested deliberately using this as a method of resolving large turbulent structures. However, to date, no one has produced a theoretical justification for this unsteady RANS (URANS) approach. Here, we extend the dynamical systems fixed point analysis of Speziale and Mhuiris [1], Girimaji et al. [2] to create a theoretical model for URANS dynamics. The results are compared to URANS simulations for homogeneous isotropic decaying turbulence. The model shows that URANS can predict incorrect decay rates and that the solution tends towards steady RANS over time. Similar analysis for forced turbulence shows a fixed modeled energy of about 30% of total energy, regardless of the model parameters. The same analysis can be used to show how hybrid type models can begin to address these issues.

1. Introduction

When Reynolds [3] introduced the averaged equations that bear his name, he posited an average that was local over a small area of space or interval of time. Inspired by an analogy to kinetic theory, he assumed that

$$\overline{\bar{u}u'} = 0, \quad (1)$$

which eliminates the cross-stress terms in the averaged equations. For kinetic theory, this is an excellent approximation: there is an extreme scale discrepancy between the mean-free path that characterizes molecular motions and the scales of interest in a continuum representation of a flow, at least for most flows of interest. For turbulence, however, which is characterized by the broad spectrum of the energy cascade, this assumption is wrong.

Subsequent literature has therefore dubbed any average a “Reynolds average”, if it has the property

$$\overline{\bar{f}\bar{g}} = \bar{f}\bar{g}, \quad (2)$$

which is a generalization of equation (1). Ironically, that makes the local spatial average Reynolds invoked not a Reynolds average, but the equations derived in Reynolds’s paper are consistent with a Reynolds average so defined. There do exist other averages that satisfy this property exactly, such as infinite time (often wrongly attributed to Reynolds), homogeneous in one or more spatial directions, or a properly constructed ensemble average.

It is evident that averages of this kind are expected to remove all turbulent scales of motion, including the very largest eddies. The earliest attempts to close these equations, such as Taylor [4], Prandtl [5], assume that the turbulence is characterized by a single set of scales, those corresponding to the largest, energy-containing eddies. This class of models, which comes to be known as RANS (Reynolds-averaged Navier-Stokes), continues to rely on the single scaling assumption. This includes $k - \varepsilon$, $k - \omega$, and Reynolds-stress models (RSM), all of which include one scaling equation which is used to obtain all the remaining unclosed quantities by a dimensional scaling. All the proposed scaling quantities (dissipation, ε , inverse time scale, ω , or length scale, among others) are assumed to be algebraically related.

With the first availability of larger computers in the 1960s, starting with the pioneering work of Smagorinsky [6], Lilly [7], Deardorff [8], turbulence modeling returned to the idea of a local spatial average over regions significantly smaller than the largest turbulent eddies. The averaging region is often identified with the computational grid cell, although they are mathematically distinct, and this conflation continues to cause confusion. This class of methods is called large-eddy simulation (LES).

The RANS literature often derives the averaged equations by invoking a long or infinite-time average, or an ensemble average, whereas LES papers typically formulate the filtered equations in terms of a local spatial filter. This has led to a widespread misunderstanding that the choice of filter used to derive the equations is what distinguishes RANS and LES. However, as Germano [9] points out, by writing the equations in terms of generalized moments, the moment equations are identical for any average, provided it is linear, and commutes with differentiation. The only difference between RANS and LES, or between any two moment closure models, for that matter, is the value of the unclosed subfilter terms. Since those terms are replaced with a closure model, it should be clear that the specific average associated with a closure is implicitly defined by the closure, rather than the opposite. This point is made very clearly by Pope [10] for the specific case of the Smagorinsky model, and what he terms the implied Smagorinsky filter, but the argument generalizes to any turbulence model.

In particular, while RANS models rely on the single scaling assumption described above, LES models invoke a cutoff scale that defines the largest scale at which the model acts. This is typically a length scale, and usually is related to the grid scale to assure maximum use of the available resolution without too large a discretization error.

It has long been known that RANS models can be used to compute time-dependent flows in cases where the model can be considered a homogeneous spatial average, for example, homogeneous isotropic decaying turbulence or the temporal spreading of a mixing layer. For these examples, the RANS equations reduce to ordinary-differential equations in the first case and partial-differential equations in time and a single space dimension in the second. Clearly, no turbulent structures are explicitly resolved. Alternatively, one might consider a flow in which the time scale of interest is very long compared to the turbulent time scale, for example, the slow spread of a contaminant plume. In addition, it has been common practice to solve for the time-steady RANS solution to a problem by using a time-dependent code and iterating in time until a steady-state is achieved.

Beginning in the 1990s, using finer grids and higher-order turbulence models and numerical schemes, RANS practitioners began to observe cases in which, for certain problems and models, simulations never reached a steady state. Instead, they observed the emergence of structures which were, at least qualitatively, similar to the large turbulent structures observed in experiments [11–13]. Numerous subsequent authors

have used RANS models to develop unsteady structures deliberately, reporting mixed success [14–19].

The results of these and other studies sometimes look promising, but raise numerous questions. First, and most fundamentally, it is not clear why some models, geometries, and initial conditions lead to unsteady solutions, while others relax to a steady solution. Second, the reported results are mixed; some authors showing relatively good agreement with experimental data, and other quite poor. This opens the question whether the more successful comparisons are purely fortuitous. At the very least, our inability to predict, a priori, when the method will work makes it impossible to rely on for engineering prediction. Finally, some quantities are easier to predict than others. Qualitative agreement between visualizations of large-scale features is not surprising, since the mechanisms that support them is often only weakly dependent on Reynolds number. For the case of shedding behind a cylinder, for example, Pereira et al. [19] propose that, since the shedding Strouhal number is only weakly dependent on Reynolds number over a wide range, it should be expected that a RANS simulation will do an adequate job of predicting it, even if the effective viscosity is poorly predicted.

Spalart [20] and Travin et al. [21] present systematic critiques of what they refer to as the unsteady RANS (URANS) approach. There is some variation in terminology between various authors. Consistent with the definitions above, we will follow the distinction made by Travin et al. [21] that LES refers to a model which includes the filter width as a parameter,¹ whereas RANS does not. We can also distinguish between VLES, which is simply an LES model that resolves a smaller portion of the spectrum than regular LES, and URANS, which is just using a traditional, unmodified RANS model but allowing the solution to become unsteady.²

Although in widespread use, a physical or mathematical justification for URANS is missing. The underlying models typically used were all developed for steady flows, with all scales modeled. The reason why unsteadiness arises in certain cases, and not in others, is not understood, other than a general idea that it is related to how unstable the flow is, and how dissipative is the model. Physical plausibility arguments for URANS seem to require a spectral gap between the large-structures and the incoherent turbulent fluctuations, which is not observed in experiment.[20,21]

The inability to specify exactly what the URANS solution is supposed to represent makes it impossible to determine if it is correct or not. Several authors have invoked a triple-decomposition, or a phase average, [11,13,17,18]. But this is an *ex post facto* reinterpretation of models that were originally derived without any accounting for large-scale resolved structures. The models are the same whether the averages in the equations are identified as ensemble averages or phase averages. In other words, there is no formal mathematical justification for interpreting the results this way. Furthermore, Spalart [20] points out that the phase-averaged structure is very different from the typical exact structure, and the resolved field is observed to include “incoherent” motions.

An alternative to URANS is to find a rational procedure for introducing an explicit decomposition parameter into a conventional RANS model. The flow-simulation methodology (FSM, [23–25]), partially-averaged Navier-Stokes (PANS, [2,22,26]) and partially-integrated transport model (PITM, [27,28]) are all examples of this approach.

¹We can slightly generalize this to include any parameter that defines the decomposition into resolved and modeled energy. The PANS approach[22], for example, parameterizes the decomposition by the fraction of energy which is modeled, rather than the cutoff length scale.

²This is consistent with the usage of Pope [10], but contrary to Spalart [20], who takes URANS and VLES as synonymous.

The emergence of these methods, which can easily be implemented in existing RANS codes, has reduced the prevalence of URANS, but has not completely replaced it.

Without a better theoretical underpinning for the URANS approach, it will remain in scientific limbo. A clear mathematical framework, on the other hand, can also help us better understand URANS in comparison with the other available modeling approaches. Travin et al. [21] writes, “Much work and discussion is needed to determine whether this situation reflects a congenital flaw, or is hiding a ‘golden opportunity’.” The goal of this paper is to present a first step in that work and discussion.

There are two primary questions to ask about URANS. First, what is the mechanism that gives rise to unsteadiness, and when does it occur? Second, in the absence of a parameter to set the scale for the energy decomposition, where does that scale come from and what value does it take? We will focus on the second question, by considering a simple test problem, and constructing an analytic model of how the energy decomposition evolves.

The test problem chosen is homogeneous isotropic turbulence, both decaying and forced. This problem is not one in which URANS is typically employed, and does not exhibit the large coherent structures seen in such geometries as bluff body wakes. In that sense, it is a particularly stringent test case. Nevertheless, it was selected for two reasons. First, it is amenable to an analytic theory which can help guide our intuitive understanding. Second, it represents the extreme in terms of lack of scale separation; if URANS can still work in this case, it should be able to work in cases with dynamically significant large structures.

2. The conventional RANS model

We start by reviewing the conventional RANS model. In the following discussion we restrict ourselves to the standard $k - \varepsilon$ model [29], although the same analysis could easily be extended to other RANS models. We decompose the velocity and pressure fields into an averaged and a fluctuating part,

$$u_i = \bar{u}_i + u'_i \quad (3a)$$

$$p = \bar{p} + p'. \quad (3b)$$

The governing equations are

$$\frac{\partial \bar{u}_i}{\partial x_i} = 0 \quad (4a)$$

$$\frac{\partial \bar{u}_i}{\partial t} + \bar{u}_j \frac{\partial \bar{u}_i}{\partial x_j} = -\frac{1}{\rho} \frac{\partial \bar{p}}{\partial x_i} - \frac{\partial R_{ij}}{\partial x_j} + \nu \nabla^2 \bar{u}_i \quad (4b)$$

$$\frac{\partial k}{\partial t} + \bar{u}_j \frac{\partial k}{\partial x_j} = \mathcal{P} - \varepsilon + \frac{\partial}{\partial x_j} \left[\left(\nu + \frac{\nu_T}{\text{Pr}_k} \right) \frac{\partial k}{\partial x_j} \right] \quad (4c)$$

$$\frac{\partial \varepsilon}{\partial t} + \bar{u}_j \frac{\partial \varepsilon}{\partial x_j} = \frac{\varepsilon}{k} (C_{\varepsilon 1} \mathcal{P} - C_{\varepsilon 2} \varepsilon) + \frac{\partial}{\partial x_j} \left[\left(\nu + \frac{\nu_T}{\text{Pr}_\varepsilon} \right) \frac{\partial \varepsilon}{\partial x_j} \right]. \quad (4d)$$

The Reynolds stress is defined as

$$R_{ij} = \overline{u'_i u'_j}, \quad (5)$$

and modeled with a linear eddy-viscosity

$$R_{ij} = -2\nu_T \bar{S}_{ij} + \frac{2}{3} k \delta_{ij}, \quad (6)$$

with

$$\bar{S}_{ij} = \frac{1}{2} \left(\frac{\partial \bar{u}_i}{\partial x_j} + \frac{\partial \bar{u}_j}{\partial x_i} \right). \quad (7)$$

The eddy-viscosity is

$$\nu_T = C_\mu \frac{k^2}{\varepsilon}, \quad (8)$$

and the production of turbulent kinetic energy is

$$\mathcal{P} = -\frac{\partial \bar{u}_i}{\partial x_j} R_{ij} = 2\nu_T \bar{S}_{ij} \bar{S}_{ij}. \quad (9)$$

The over-bar represents an average, which is often taken to be a homogenous spatial average, for problems with one or more homogeneous spatial dimensions, or a time average, for steady problems. For more general problems, it is common to invoke an ensemble average. These averages are often equivalent, assuming ergodicity holds. The turbulent kinetic energy,

$$k = \frac{1}{2} \overline{u'_i u'_i}, \quad (10)$$

and the dissipation rate,

$$\varepsilon = \nu \overline{\frac{\partial u'_i}{\partial x_j} \frac{\partial u'_i}{\partial x_j}}, \quad (11)$$

are then the energy and dissipation in the scales of motion too small to be resolved in the \bar{u}_i velocity field.

In fact, the exact averaged equations, which these equations are a model for, are identical, regardless of which average is invoked. This implies that the average that is obtained from an actual simulation is a consequence of the specific model closure used, and is independent of the average specified by the author, if any. In the case of the $k-\varepsilon$ model, the average is implied by the modeling assumption that the eddy-viscosity can be scaled with a velocity characteristic of the entire turbulent motion, $k^{1/2}$, and a length-scale

$$L \sim \frac{k^{3/2}}{\varepsilon},$$

as well as the rescalings that go into modeling the dissipation rate. Consistent with our definitions in section §1, the RANS has no explicit parameter defining a partition of resolved and modeled scales. An alternative closure approach would be to explicitly introduce such a parameter to obtain an LES model. For example, if we impose a length

scale for computing the eddy-viscosity, $L \sim C_S \Delta x$, then the equations are immediately closed without the need for a dissipation rate equation (4d), and we recover the one-equation LES model of Schumann [30], Yoshizawa [31].

Particular care must be given to initial and boundary conditions. Equations (4) allow for injecting both a modeled and a resolved component of turbulent fluctuations through the initial and boundary conditions. There is nothing in the equations, however, which ensures that this injection is consistent with the energy decomposition implied by the model. In fact, it is fair to ask whether the possibility of forcing the model in an inconsistent manner constitutes a defect in the model, or just a caveat on how we treat initial and boundary conditions.

Applying equations (4) to homogeneous isotropic decaying turbulence, using the conventional RANS approach, we assume that the average removes all the turbulent scales. Since the flow is statistically homogeneous, all the average quantities are uniform in space, and the equations reduce to ordinary differential equations. To indicate this, we will replace the over-bar with an angle bracket. This could represent a spatial average over all of space, or an ergodically equivalent, suitably constructed, ensemble average. The average velocities are identically zero, $\langle u_i \rangle = 0$, and the $k - \varepsilon$ equations reduce to a set of ordinary differential equations,

$$\frac{d\langle k \rangle}{dt} = -\langle \varepsilon \rangle \tag{12a}$$

$$\frac{d\langle \varepsilon \rangle}{dt} = -C_{\varepsilon 2} \frac{\langle \varepsilon \rangle^2}{\langle k \rangle}. \tag{12b}$$

The solution to this problem is well known to be

$$\langle k \rangle = k_0 \left(\frac{t}{t_0} \right)^{-n}, \tag{13}$$

where the decay rate is

$$n = \frac{1}{C_{\varepsilon 2} - 1}. \tag{14}$$

For this simple RANS model, the decay rate is a constant. Data from experiments and simulations suggest that this may not be quite right, but for a particular experiment, over a wide range of Reynolds number, it is a reasonable approximation [32,33].

3. Unsteady RANS

We can also try to simulate this problem using a URANS. This means we use the same $k - \varepsilon$ RANS equations (4), but now we include all the unsteady and locally varying terms. For this problem, unsteadiness will not arise spontaneously, so we need to introduce it through the choice of initial conditions. We wish to do so in a way that is consistent with the idea that the initial conditions represent some suitably averaged real turbulent state. In practice, we can achieve this by computing a fully resolved turbulent field using direct-numerical simulation of the unfiltered Navier-Stokes equations. The simulation is allowed to evolve until the flow reaches the asymptotic state of homogeneous decay. We then choose a low-pass filter with a specified length-scale.

The velocities can be filtered directly, and the turbulence quantities can be obtained using equations (10) and (11).

The governing equations are now

$$\frac{\partial \bar{u}_i}{\partial x_i} = 0 \quad (15a)$$

$$\frac{\partial \bar{u}_i}{\partial t} + \bar{u}_j \frac{\partial \bar{u}_i}{\partial x_j} = -\frac{1}{\rho} \frac{\partial \bar{p}}{\partial x_i} + \frac{\partial}{\partial x_j} \left[\left(\nu + \nu_T^< \right) \left(\frac{\partial \bar{u}_i}{\partial x_j} + \frac{\partial \bar{u}_j}{\partial x_i} \right) \right] \quad (15b)$$

$$\frac{\partial k_{<}}{\partial t} + \bar{u}_j \frac{\partial k_{<}}{\partial x_j} = \mathcal{P}_{<} - \varepsilon_{<} + \frac{\partial}{\partial x_j} \left[\left(\nu + \frac{\nu_T^<}{\text{Pr}_k^<} \right) \frac{\partial k_{<}}{\partial x_j} \right] \quad (15c)$$

$$\frac{\partial \varepsilon_{<}}{\partial t} + \bar{u}_j \frac{\partial \varepsilon_{<}}{\partial x_j} = \frac{\varepsilon_{<}}{k_{<}} (C_{\varepsilon 1}^< \mathcal{P}_{<} - C_{\varepsilon 2}^< \varepsilon_{<}) + \frac{\partial}{\partial x_j} \left[\left(\nu + \frac{\nu_T^<}{\text{Pr}_\varepsilon^<} \right) \frac{\partial \varepsilon_{<}}{\partial x_j} \right], \quad (15d)$$

with

$$\mathcal{P}_{<} = 2\nu_T^< \bar{S}_{ij} \bar{S}_{ij},$$

and

$$\nu_T^< = C_\mu \frac{k_{<}^2}{\varepsilon_{<}}.$$

Note, these equations are formally identical to the RANS equations (4), however, we have introduced super- or subscript less-than decorations to various quantities to emphasize that they now represent subfilter quantities. Both the velocities and the turbulence quantities now vary in both time and space.

The bar now represents a local *filter*, which does not remove all turbulent scales, and the term *average*, denoted by angle brackets will be reserved for the homogeneous average over the entire box. It is important to note that, as mentioned above, the filter corresponding to a specific model is implicitly defined by the model, and is therefore not known in a closed form that can be used to compute the initial conditions. We will assume that the effect of using slightly different low-pass filters leads to, at most, minimal, short-lived transients as the flow adjusts.

Unlike LES models, which have an explicit cut-off length scale specified, when using a conventional RANS model to try to compute unsteadiness, the model does not include a parameter that controls which scales, or how much of the energy, is to be captured by the model. This makes it difficult to say what constitutes the correct answer. Instead we will focus on two questions. How does the partition of energy between resolved and model scales evolve? And, how well does the URANS predict the overall decay rate? The first question addresses how useful the model is: given that we do not control the energy partition, does it behave in a manner that produces an informative result? The second question is more about correctness. There may not be a clear right answer for each component, resolved and modeled, of the energy, but the total energy should give something like a power-law decay, as observed in experiments, with at most a slowly varying decay rate. In particular, if the energy partition changes, it should do so in a way that does not degrade the solution for the total energy.

In order to explore these questions, it would be nice if we could reduce equations (15) to a set of ordinary differential equations. We could then employ the dynamical systems and fixed point analysis first introduced by Speziale and Mhauris [1] in the steady RANS

context, and applied to URANS by Girimaji et al. [2]. In their approach, they omitted the unsteady transport term as not contributing to the global energy balance. We take a slightly different approach and formally average the unsteady equations. To do this, we first introduce the decomposition

$$k = \langle k_{>} \rangle + \langle k_{<} \rangle,$$

where

$$k_{<} = \frac{1}{2} (\overline{u_i u_i} - \bar{u}_i \bar{u}_i) \quad (16a)$$

$$k_{>} = \frac{1}{2} (\bar{u}_i \bar{u}_i - \langle \bar{u}_i \rangle \langle \bar{u}_i \rangle), \quad (16b)$$

are the energy of the subfilter and resolved scales, respectively. This decomposition requires the assumption that $\langle \bar{f} \rangle \approx \langle f \rangle$. This can be demonstrated explicitly for certain filters and averages. A similar decomposition exists for the dissipation.

Taking the average of equation (15c) and using homogeneity, the equation for the subfilter energy is exactly

$$\frac{\partial \langle k_{<} \rangle}{\partial t} = \langle \mathcal{P}_{<} \rangle - \langle \varepsilon_{<} \rangle. \quad (17)$$

The equation for the average resolved energy can be derived by multiplying equation (15b) by \bar{u}_i , and averaging,

$$\frac{\partial \langle k_{>} \rangle}{\partial t} = -\langle \mathcal{P}_{<} \rangle - \langle \varepsilon_{>} \rangle. \quad (18)$$

The subfilter dissipation equation (15d), when averaged, yields

$$\frac{\partial \langle \varepsilon_{<} \rangle}{\partial t} = C_{\varepsilon 1}^< \left\langle \frac{\varepsilon_{<}}{k_{<}} \mathcal{P}_{<} \right\rangle - C_{\varepsilon 2}^< \left\langle \frac{\varepsilon_{<}^2}{k_{<}} \right\rangle. \quad (19)$$

This is an exact equation for how the subfilter dissipation rate will evolve under the action of the RANS model given by equation (4). In order to solve this equation, an additional level of closure modeling is required, since the two averaged terms on the right-hand side are not closed. That is, this equations includes a closure model relative to the bar filter, but still requires closing relative to the bracket filter. The simplest model for equation (19) is

$$\left\langle \frac{\varepsilon_{<}^2}{k_{<}} \right\rangle \approx \frac{\langle \varepsilon_{<} \rangle^2}{\langle k_{<} \rangle} \quad (20)$$

$$\left\langle \frac{\varepsilon_{<}}{k_{<}} \mathcal{P}_{<} \right\rangle \approx \frac{\langle \varepsilon_{<} \rangle}{\langle k_{<} \rangle} \langle \mathcal{P}_{<} \rangle. \quad (21)$$

This is correct to second order in the fluctuations [34]. For the remaining unclosed

quantities, we use

$$\langle \mathcal{P}_< \rangle \approx \langle \nu_T \rangle \langle \bar{\omega}^2 \rangle \quad (22)$$

$$\langle \varepsilon_> \rangle = \nu \langle \bar{\omega}^2 \rangle, \quad (23)$$

where we also decompose the average eddy-viscosity as

$$\langle \nu_T \rangle = C_\mu \frac{\langle k_< \rangle^2}{\langle \varepsilon_< \rangle}. \quad (24)$$

Note that equation (23) is exact, whereas equation (22) neglects the spatial variation of the eddy-viscosity.

We can now close the three equations (17), (18) and (19) by adding an evolution equation for filtered enstrophy magnitude, $\langle \bar{\omega}^2 \rangle$. To obtain this we start by noting that the dissipation equation (12b) is essentially an enstrophy equation,

$$\frac{d \langle \omega^2 \rangle}{dt} = -C_{\varepsilon 2} \frac{\nu \langle \omega^2 \rangle^2}{\langle k \rangle}. \quad (25)$$

If we assume that the dynamics of a URANS simulation can be modeled as a Navier-Stokes simulation with a reduced viscosity of ν_T , rather than ν , then a plausible model for the enstrophy of the resolved scales is

$$\frac{\partial \langle \bar{\omega}^2 \rangle}{\partial t} = -C_{\varepsilon 2}^> \frac{\langle \nu_T \rangle \langle \bar{\omega}^2 \rangle^2}{\langle k_> \rangle}. \quad (26)$$

(A similar argument can be found in [10] for deriving an estimate of the filtered spectrum produced by an LES model.)

The coefficient $C_{\varepsilon 2}^>$ plays the same role for the enstrophy dissipation of the filtered scales as the $C_{\varepsilon 2}^<$ plays for the subfilter scales in the original RANS model, and is the only parameter of the reduced order model. The parameters $C_{\varepsilon 1}^<$ and $C_{\varepsilon 2}^<$ are not tunable parameters of the reduced order model, they must be set to whatever the values are used in the URANS simulations we are comparing to. For the results presented here, the value used is the standard $C_{\varepsilon 2}$ parameter setting, $C_{\varepsilon 2}^> = 1.92$.

The complete set of modeled equations is now

$$\frac{\partial \langle k_> \rangle}{\partial t} = -\langle \mathcal{P}_< \rangle - \langle \varepsilon_> \rangle \quad (27a)$$

$$\frac{\partial \langle \bar{\omega}^2 \rangle}{\partial t} = -C_{\varepsilon 2}^> \frac{\langle \nu_T \rangle \langle \bar{\omega}^2 \rangle^2}{\langle k_> \rangle} \quad (27b)$$

$$\frac{\partial \langle k_< \rangle}{\partial t} = \langle \mathcal{P}_< \rangle - \langle \varepsilon_< \rangle \quad (27c)$$

$$\frac{\partial \langle \varepsilon_< \rangle}{\partial t} = \frac{\langle \varepsilon_< \rangle}{\langle k_< \rangle} (C_{\varepsilon 1}^< \langle \mathcal{P}_< \rangle - C_{\varepsilon 2}^< \langle \varepsilon_< \rangle). \quad (27d)$$

The first thing to note about these equations is that if we sum equations (27a) and (27c), we recover the exact total energy equation (12a). (This is, in fact, a property of the exact unclosed equations, so will hold for any closure model.) It is evident that

the subfilter production term, $\langle \mathcal{P}_< \rangle$ represents the transfer of energy from the resolved to the subfilter scales. As such, it is the primary term which sets the decomposition scale. This point is widely misunderstood, and bears emphasis. *The decomposition into resolved and subfilter components is not unique, and the partition of energy is set implicitly by the model through the action of $\langle \mathcal{P}_< \rangle$.*

Summing equation (27d) and viscosity times (27b) does not recover the total dissipation equation (12b), however. Instead we obtain

$$\frac{\partial \varepsilon}{\partial t} = \left(C_{\varepsilon 1}^< \frac{\langle \varepsilon_< \rangle}{\langle k_< \rangle} - C_{\varepsilon 2}^> \frac{\langle \varepsilon_> \rangle}{\langle k_> \rangle} \right) \langle \mathcal{P}_< \rangle - C_{\varepsilon 2}^< \frac{\langle \varepsilon_< \rangle^2}{\langle k_< \rangle} \quad (28)$$

If we assume that the corresponding terms play similar roles in the dissipation equations as they do in the kinetic energy equations, then the first two term represent the dissipation of enstrophy out of the large scales, and into the small scales, and should therefore cancel. The last term should represent the dissipation of small scale dissipation, and should equal the right-hand side of equation (12b). That this is not the case allows our model for the URANS to explore deviations from the RANS power law decay. This is in distinction from the analysis of Girimaji et al. [2], which assumes the total dissipation still obeys equation (12b).

Rather than analyzing the full set of equations (27), we can construct a reduced order model in terms of the primary quantities of interest. The first of these is the energy partition, defined as

$$f = \frac{\langle k_< \rangle}{k}. \quad (29a)$$

The equation for this quantity can be written in terms of two other quantities, the subfilter production to dissipation ratio, and the subfilter Reynolds number,

$$g = \frac{\langle \mathcal{P}_< \rangle}{\langle \varepsilon_< \rangle} \quad (29b)$$

$$R = \frac{\langle \nu_T \rangle}{\nu}, \quad (29c)$$

to form a closed set,

$$\frac{df}{dt^*} = (R^{-1}fg + f + g - 1) f \quad (30a)$$

$$\frac{dg}{dt^*} = 2(C_{\varepsilon 2}^< - 1)g - \left(C_{\varepsilon 2}^> \frac{f}{1-f} + 2(C_{\varepsilon 1}^< - 1) \right) g^2 \quad (30b)$$

$$\frac{dR}{dt^*} = ((2 - C_{\varepsilon 1}^<)g + C_{\varepsilon 2}^< - 2)R. \quad (30c)$$

To fully non-dimensionalize the system, we have introduced the non-dimensional time

$$\frac{dt}{dt^*} = \frac{\langle k_< \rangle}{\langle \varepsilon_< \rangle}. \quad (31)$$

This model has a singularity at when the subfilter Reynolds number goes to zero, but for even moderate Reynolds number, the singular term is negligible, and the f and

g equations evolve independently of R . We can better understand the behavior of R by noting that

$$R = C_\mu \frac{g + R}{R} f^2 \text{Re}_t,$$

where the turbulent Reynolds number is defined as,

$$\text{Re}_t = \frac{k^2}{\nu \varepsilon}. \quad (32)$$

Therefore the singular term behaves as

$$R^{-1} f g = C_\mu^{-1} \frac{R}{g + R} \frac{g}{f} \text{Re}_t^{-1}.$$

This term will blow up in two situations. The first is when $\text{Re}_t \rightarrow 0$, that is, when the turbulence is almost completely dissipated. We can neglect this case as uninteresting to our current investigation. The second is when $f \rightarrow 0$, which is the DNS limit, when the flow is almost completely resolved. For this latter situation, for this term to be $\mathcal{O}(1)$, we must have $f \sim \text{Re}_t^{-1}$. This case can also be ignored, since if f was that small, we would just run DNS instead of URANS. Consequently, the reduced-order model can be well approximated as

$$\frac{df}{dt^*} = (f + g - 1) f \quad (33a)$$

$$\frac{dg}{dt^*} = 2(C_{\varepsilon_2}^< - 1)g - \left(C_{\varepsilon_2}^> \frac{f}{1-f} + 2(C_{\varepsilon_1}^< - 1) \right) g^2. \quad (33b)$$

The same equations can be obtained directly by neglecting the viscous dissipation in the resolved scales, $\langle \varepsilon_{>} \rangle$, in equation (27a).

This model has four fixed points,

$$f = 0 \quad g = 0 \quad (34a)$$

$$f = 0 \quad g = \frac{C_{\varepsilon_2}^< - 1}{C_{\varepsilon_1}^< - 1} \quad (34b)$$

$$f = 1 \quad g = 0 \quad (34c)$$

$$f = \frac{2C_{\varepsilon_1}^< - 2C_{\varepsilon_2}^<}{2C_{\varepsilon_1}^< - C_{\varepsilon_2}^> - 2} \quad g = \frac{2C_{\varepsilon_2}^< - C_{\varepsilon_2}^> - 2}{2C_{\varepsilon_1}^< - C_{\varepsilon_2}^> - 2}. \quad (34d)$$

The last one is an attractor that governs the behavior of the system. As can be seen in figure 1, all trajectories tend towards this fixed point, which is very near the RANS limit.

For comparison, figure 1 also shows several real trajectories from numerical experiments, in red. To obtain these, a fully resolved DNS simulation for forced homogeneous turbulence was run until it reached equilibrium. The velocity fields obtained were filtered (as described above) to obtain initial conditions for the URANS. Each trajectory was created using a different filter width to generate the initial condition. The trajectory was then computed using a URANS. Details of the simulations can be found in [35].

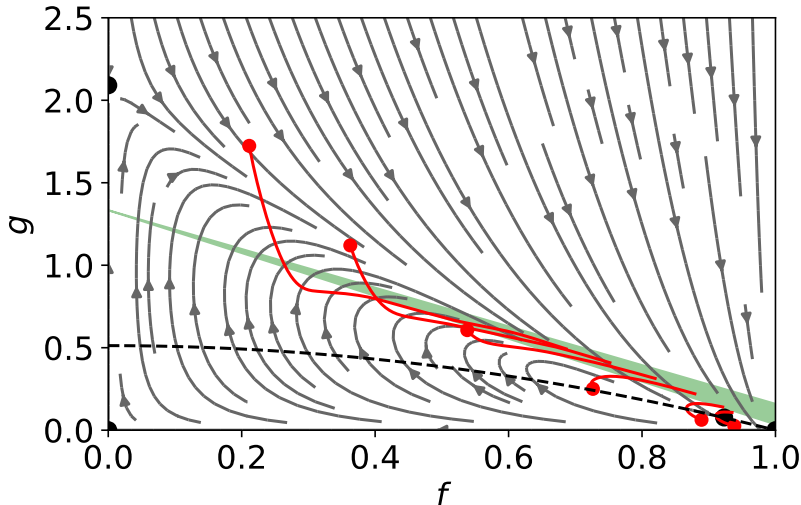


Figure 1. Phase space evolution of equation (33). The grey trajectories are the reduced order model, with the fixed points in black. Red lines are trajectories from simulation data (with points indicating the beginning of each trajectory). The green shaded region is where $n = 1.15 - 1.45$. The dashed curve is equation (A12).

What the figure clearly shows is that, regardless of the initial condition, the URANS evolves towards something very like a steady RANS, with the resolved fluctuations decaying away. The model suggests that the URANS will not go all the way to the RANS limit of $f = 1$, however the data is not sufficient to determine if this is the case. What is clear, is that the user has no control over the range of scales which are physically resolved. However, it should be noted that the rate at which the URANS relaxes towards RANS is extremely slow in turbulence time scales, which may be one reason why some URANS practitioners are left with the impression that the initial choice of energy partition persists.

Having considered the evolution of the energy partition, we now examine the decay rate of the total turbulent kinetic energy. For a flow in which the decay rate may be changing, there are several ways to measure this [36]. We choose

$$n = \left(\frac{d}{dt} \left[\frac{k}{\varepsilon} \right] \right)^{-1}, \quad (35)$$

which has the advantage that it can be computed from equations (27) in terms of our reduced order model,

$$n = \frac{f}{C_{\varepsilon 2}^< - C_{\varepsilon 1}^< g - f}. \quad (36)$$

On our trajectory plot, curves of constant n are straight lines through the point $f = 0$, $g = C_{\varepsilon 2}^< / C_{\varepsilon 1}^<$. The green shaded region in figure 1 is where the decay matches the observed range of experimental data, $n = 1.15 - 1.45$.

It is clear that the shaded region, where the decay rate matches experiment, occupies only a small fraction of phase space. Whether this is a problem for the URANS approach in practice depends largely on how much time the URANS spends outside this small

region. The plotted trajectories suggest that the URANS does evolve to this region, given sufficient time. Another question might be, where do typical initial conditions fall relative to this region. For example, given a local spatial filter, characterized by a cutoff length-scale, we could filter DNS data at various cutoffs, to obtain an initial condition for each one. Each initial condition would define one point in phase space, and the points for all possible filter widths would define a curve. We can approximate that curve using a stick-spectrum analysis, to obtain the dashed curve, equation (A12), shown in figure 1. (The details of the derivation are given in section §A). From this analysis, it appears that the initial conditions thus produced fall well below the shaded region, meaning they will be a significant adjustment before the correct energy decay rate is observed. The red trajectories, on the other hand, start well above (at least for small f), the difference probably being a result of the specific way they are generated, starting with a forced turbulence and only later being allowed to decay, as described in [35].

An interesting feature of the reduced-order model is that if we use equation (34d) and equation (36) to compute the decay rate at the fixed point, we get

$$n = \frac{2}{C_{\varepsilon 2}^>} \quad (37)$$

In other words, the decay rate is independent of the underlying RANS model, and is a function of the dynamics of the resolved scales alone. The model coefficient we chose predicts a decay rate of $n \approx 1.02$, noticeably lower than might be expected from experiments. However, from equation (36) we see that changing $C_{\varepsilon 2}^>$ does not actually change the decay rate at any point in phase space, rather it moves the fixed point itself. In fact, lowering $C_{\varepsilon 2}^>$ much beyond the value adopted here moves the fixed point outside of the allowable range $0 \leq f \leq 1$, so that the $f = 1$ fixed point becomes the attractor.

A similar factor explains why we cannot adjust the model to lower the fixed point on the upper-left, to try to improve the fit. The location of this point is controlled by the URANS model coefficients $C_{\varepsilon 1}^<, C_{\varepsilon 2}^<$, which are not adjustable parameters of the reduced-order model, and must be set to match the coefficients settings used in the URANS we are comparing to.

Another way we can assess the accuracy of the model is to compare the measured growth rate in the simulations to the model prediction using equation (36) with f and g computed from the simulation data. This is shown in figure 2. If the model was perfect, all the data would fall on the dashed line. As is clear from the plot, for some of the trajectories (specifically, the ones with higher f), the agreement is excellent. For the trajectories closer to DNS, the agreement is not as good; the relationship is still linear, but the measured decay rate is about 30% high. Also, for those trajectories for which we observe a kink in the track in figure 1, the scaling relationship in figure 2 seems to be different before and after the kink.

Overall, the reduced order model equation (33) gives us a good feel for the dynamics of the URANS. We can see that the solution can deviate substantially from the correct decay rate as it evolves. However, there appears to be a preferred trajectory, a roughly straight path between two of the fixed points (on the upper-left and lower-right in figure 1), along the lower portion of which the decay rate is close to the experimental values. This may give a false sense that the URANS approach is correct. At least from the reduced-order model, it appears that the preferred trajectory is not aligned with a contour of constant decay rate, although the full simulation trajectories are less clear.

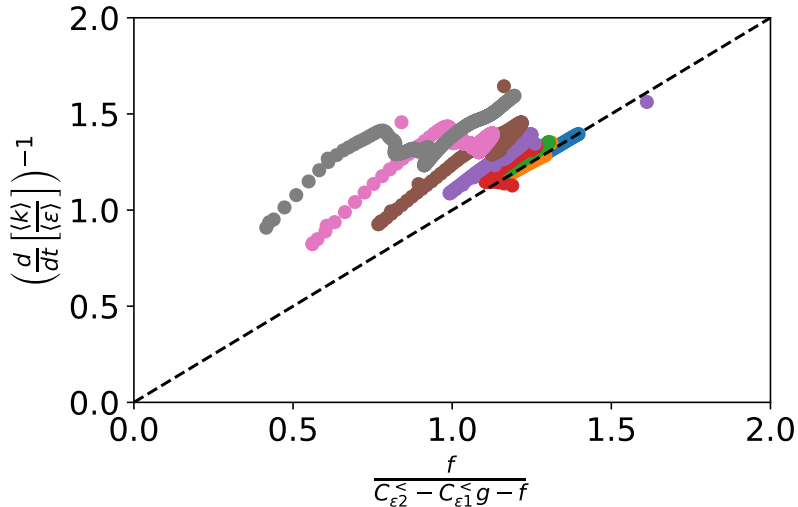


Figure 2. The measured decay rate compared versus the decay rate predicted by the model (equation 36) for the URANS simulations [35].

4. Forced Turbulence

Decaying turbulence is arguably not analogous to problems, such as bluff body wakes, in which unsteadiness arises spontaneously in URANS. It is more similar to problems where the initial condition includes a resolved perturbation or geometric feature that creates an initial large-scale structure which decays over long times, such as[37,38]. For the wake, where the flow is globally unstable, the instability acts as a kind of forcing term which sustains the unsteadiness in the URANS solution. The equivalent mechanism for homogeneous turbulence would be forced turbulence, which we consider in this section.

Consider a DNS of homogeneous isotropic turbulence generated by a large scale forcing. The flow evolves under a statistically stationary stochastic forcing until statistical equilibrium is reached. At this point, as for the decaying problem, the flow is decomposed into resolved and subfilter quantities using a specified cutoff length-scale. The problem is then restarted, using the URANS equations, initialized with the resolved and modeled fields, and the evolution is continued with the same forcing. This is again repeated with a series of different cutoffs.

To model this problem, we will make the following assumptions. First, that the forcing is entirely in the resolved component, regardless of the cutoff length-scale. Second, that the flow remains in equilibrium, so that we can assume that the forcing is always balanced by the dissipation, $\mathcal{F} = \varepsilon$. Finally, that the forcing does not directly effect the dissipation or enstrophy. In that case, equations (27b), (27c) and (27d) remain unchanged, however equation (27a) becomes

$$\frac{\partial \langle k \rangle}{\partial t} = - \langle \mathcal{P} \rangle - \langle \varepsilon \rangle + \mathcal{F},$$

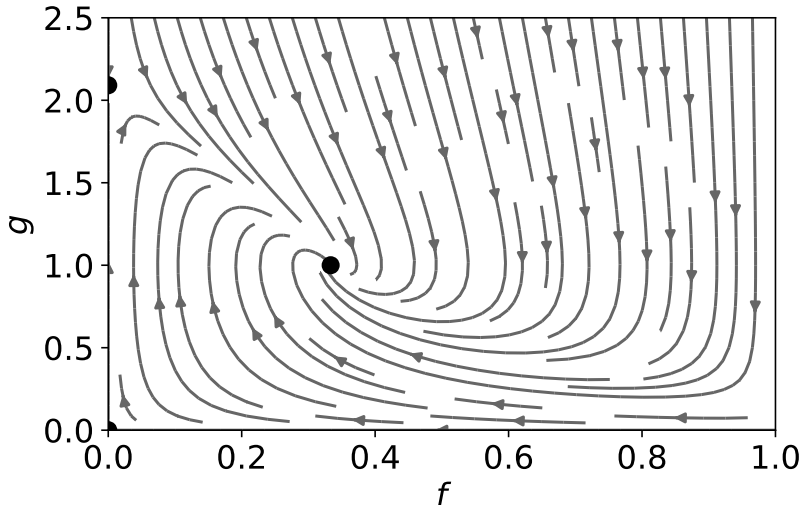


Figure 3. Phase space evolution for homogeneous forced turbulence, equations (38) and (30b). The grey trajectories are the reduced order model, with the fixed points in black.

and

$$\frac{dk}{dt} = 0.$$

The reduced-order model for the forced case is, therefore

$$\frac{df}{dt^*} = f(g - 1), \quad (38)$$

and the g equation is still equation (30b). The fixed points are

$$f = 0 \quad g = 0 \quad (39a)$$

$$f = 0 \quad g = \frac{C_{\varepsilon 2}^< - 1}{C_{\varepsilon 1}^< - 1} \quad (39b)$$

$$f = \frac{2(C_{\varepsilon 1}^< - C_{\varepsilon 2}^<)}{2C_{\varepsilon 1}^< - 2C_{\varepsilon 2}^< - C_{\varepsilon 2}^>} \quad g = 1 \quad (39c)$$

With the standard $k - \varepsilon$ coefficients, this results in an attracting fixed point at $g = 1$ and $f \approx 0.3$, as can be seen in figure 3.

Unlike the unforced case, the energy partition does not trend towards a steady RANS solution in the forced case. Instead, the forcing acts as a continuous source of resolved scale energy. The fixed point represents the balance between the dissipation of resolved scale motion due to the model and the production of resolved scale motion due to the forcing. A value of $g = 1$ at the fixed point means that the energy input due to forcing is the same as the transfer (production) between resolved and subfilter scales, which is the same as the subfilter dissipation, that is, a classic cascade process. The fixed points we obtain are different from those in [2] because we do not assume that the total dissipation rate follows the steady RANS equation, as we describe above.

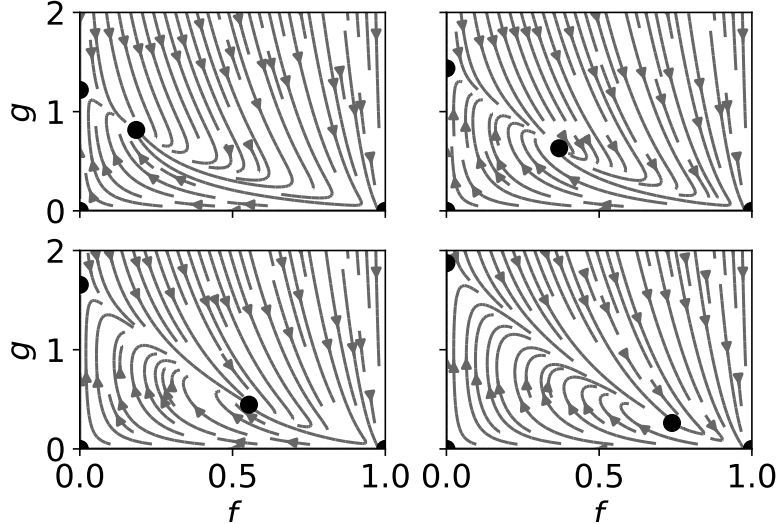


Figure 4. Phase space evolution of unforced PANS with different values of f_k . From top left, $f_k = 0.2, 0.4, 0.6, 0.8$.

5. Implications for RANS based hybrid models

The fundamental problem with the URANS approach is that, regardless of how the simulation is initialized, conventional RANS model equations are designed to account for all the turbulent scales of motion. When used to simulate only a range of scales, the dynamics of the solution fundamentally disagrees with the modeling assumptions. In order to fix this problem, there exists a class of hybrid turbulence models which, through various mathematical procedures, attempt to rescale the subfilter quantities in the RANS equations to properly account for the partition between resolved and modeled scales. These include the flow-simulation methodology (FSM) [23,25], partially averaged Navier-Stokes (PANS) [2,22], and the partially integrated transport model (PITM) [28]. The reduced-order model approach from the previous section is easily extended to these hybrid models. In fact, for models where the only change is a modification to the model coefficients, the reduced-order model (30) still applies, it only needs to be replotted with the appropriate coefficient values.

To demonstrate this, we consider the PANS model. In the PANS approach, the $C_{\varepsilon 2}^<$ coefficient is replaced with a rescaled version,

$$C_{\varepsilon 2}^* = f_k (C_{\varepsilon 2}^< - C_{\varepsilon 1}^<) + C_{\varepsilon 1}^<, \quad (40)$$

f_k is a model parameter that is supposed to set the ratio of the modeled to total energy. This is distinguished from f , which is the actual ratio achieved by the simulation. In other words, f_k is an input to the model, and f is a diagnostic; if the PANS model worked exactly as intended, f_k and f would be equal.

Figure 4 shows the trajectory maps for the PANS models with four different values of f_k . The fixed points move depending on f_k , and the behavior is as desired: as f_k decreases, the value of f at the attracting fixed point also decreases. We can substitute $C_{\varepsilon 2}^*$ from (40) for $C_{\varepsilon 2}^<$ in the expression for the reduced-order model fixed point value

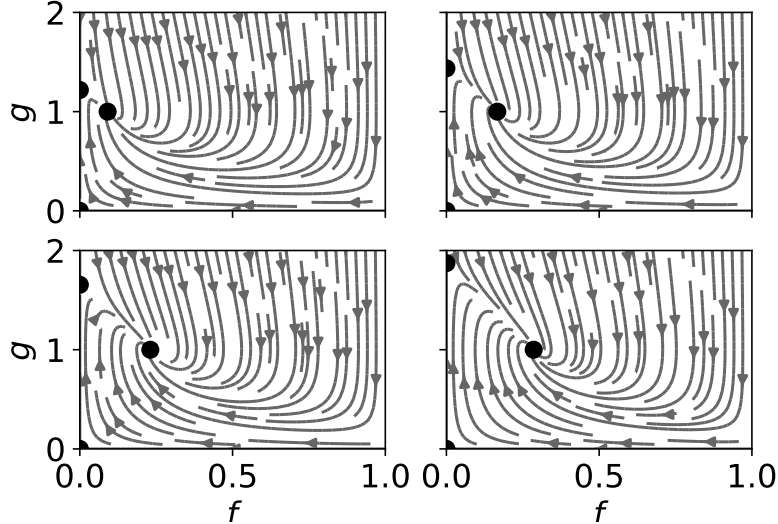


Figure 5. Phase space evolution for forced PANS with different values of f_k . From top left, $f_k = 0.2, 0.4, 0.6, 0.8$.

of f , (34d), to obtain an analytic relationship between f_k and f at the fixed point,

$$f = \frac{2(C_{\varepsilon 1}^< - C_{\varepsilon 2}^<)}{2C_{\varepsilon 1}^< - C_{\varepsilon 2}^> - 2} f_k. \quad (41)$$

For the standard values of the model coefficients, this is approximately $f \approx 0.96 f_k$, which is very close to the desired equality. Note also, that from equation (37), the growth rate at the fixed point is independent of f_k .

We can conduct the same experiment for the forced case. In this case, we do not expect the result to relax to a steady solution in the limit of $f_k \rightarrow 1$, since the underlying RANS model does not do so. Instead, the level of unsteadiness is restricted to range of $f \approx 0 - 0.3$, as can be seen in figure 5.

In other words, for the unforced case, the PANS model does exactly what it is designed to do. Unlike URANS, where the limiting behavior relaxes to a conventional RANS, the PANS model tends towards a value of f very close to the value of the input parameter f_k . Nevertheless, it is important to be aware that the PANS model also can have significant deviations from the fixed point, particularly if the initial condition is not chosen so that both f and g are at the fixed point value for the specified f_k . For the forced case, the relationship between the input f_k and the observed f is more complex. Obviously, the PANS model cannot enforce a steady result at the $f_k = 1$ limit if the underlying RANS model cannot.

6. Conclusions

Conventional RANS models were developed using a single-scale assumption. Such closures are only justified where any resolved unsteadiness exhibits a “spectral gap,” or, equivalently, the large scales, such as the total turbulent kinetic energy and the integral length scale, completely characterize the turbulence. Even for problems with

large unsteady turbulent structures, these models were designed to produce the correct solution for the time mean, when solved for the steady-state solution (i.e., when the time-derivative terms are set to zero). Proponents of the URANS approach have not produced a rigorous justification as to why these models sometimes give rise to unsteady solutions if allowed to evolve in time, nor what precisely those unsteady solutions represent. Without clearly identifying what the models should do, it is hard to say definitely whether the results they do produce are correct or not, or even what would be the correct way to employ them.

One key limitation in our understanding is that existing research into URANS consists of case studies. Even very careful analysis can lead to uncertain, and even contradictory, conclusions, given the enormous parameter space of all potential applications of URANS. What has been missing is a theoretical framework for understanding what URANS actually does. This paper presents a first step in that direction.

The proposed model can be viewed as an extension of earlier fixed point analyses. The power of the approach lies in viewing the evolution of the URANS simulation as a dynamical system, with the phase space dynamics giving insight into the global behavior of the model. The purpose of the model is not to be an accurate predictive tool, but rather to reproduce the qualitative behaviors we expect to see in URANS simulations. Comparisons to actual simulation data indicates that the model does just that.

Without a clear metric for correctness, it is impossible to say definitively that URANS is wrong, but these results show that the idea that a steady RANS model can simply be applied to unsteadiness and a correct answer obtained is a myth. Defenders of the URANS approach might try to argue that the results in figure 1, showing that the URANS has a preference for trajectories that fall near the region of correct decay rate, vindicates the approach. However, there are three serious difficulties with this view. First, the fact that a URANS solution will decay in time until almost all resolved scales are dissipated and a steady RANS solution is achieved, is neither a useful model behavior, nor consistent with most users expectations for an unsteady model. Second, both the stick spectrum analysis and the simulation data initialized with forced turbulence show that initializing the URANS so that it starts in a state where the decay rate is reasonable is not a trivial undertaking. Finally, while the model may, in certain cases, predict the decay rate properly, in others it can undergo extreme transients into highly non-physical behaviors.

Extending the analysis to the hybrid PANS model, we see that for decaying turbulence PANS solves the first of these issues, placing the fixed point at exactly the resolution the user requested. However, the path to the fixed point, and, in particular, inconsistent initial conditions, still are issues that require further study. Here too, the forced case show more complicated dynamics. This is consistent with the observation that the hybrid model cannot be calibrated to enforce an energy partition more coarse than the underlying RANS model upon which it is built.

The approach does need to be extended to more common applications of URANS. Work is underway for an extension to free shear and mixing layers. In the meantime, the case of forced turbulence provides a possible analog for the mechanisms at work in URANS of globally unstable flows, with the forcing acting as a proxy for the global instability. These results show that in such a case the forcing can keep the unsteadiness alive. The energy partition is controlled by a balance between the model damping and the forcing input.

In either case, further analysis would be served by the proponents of the URANS approach clearly defining metrics for what they believe the correct behavior of the

model should be. In the meantime, users of models would be advised to have a very clear understanding of what can and cannot be expected of RANS models before applying them to unsteady problems.

Acknowledgements

The author would like to express his gratitude to Dr. Colin Towery for providing simulation data for comparison, as well as very helpful discussions. Thanks also to Dr. Filipe Pereira for his insightful comments on the manuscript. This research was funded by the LANL Mix and Burn project under the DOE ASC, Physics and Engineering Models program.

Appendix A. Stick spectrum analysis

The initial conditions for a URANS type simulation (or, equivalently, for a PANS/hybrid/SRS simulation) cannot fall in any arbitrary point in f, g, R space. The production-to-dissipation ratio, g , will depend on the energy partition, f . Another way to look at it is, given a particular filter that is parameterized by a length scale, ℓ , for each ℓ we will have specific values of f , g , and R . That is, $f = f(\ell)$, $g = g(\ell)$, and $R = R(\ell)$ are all functions of ℓ . Choosing a different filter shape will result in a slightly different curve, but it is likely that this will be a weak effect.

We can estimate this dependence by using an assumed spectrum analysis [39, and references therein]. If we take L as the characteristic length scale of the large scales, and the Kolmogorov scale, η , as characterizing the smallest scales, we can use an assumed spectrum of

$$E(\kappa) = \begin{cases} C \langle \varepsilon \rangle^{2/3} \kappa^{-5/3} & \kappa \in [2\pi/L, 2\pi/\eta] \\ 0, & \text{elsewhere} \end{cases}. \quad (\text{A1})$$

The subfilter turbulent kinetic energy is

$$\langle k_{<} \rangle = \int_{\frac{2\pi}{\ell}}^{\infty} E(\kappa) d\kappa. \quad (\text{A2})$$

Integrating the assumed spectra equation (A1) gives an estimate of

$$\langle k_{<} \rangle = \frac{3}{2} C \langle \varepsilon \rangle^{2/3} \left(\frac{\ell}{2\pi} \right)^{2/3} \left[1 - \left(\frac{\eta}{\ell} \right)^{2/3} \right]. \quad (\text{A3})$$

The total turbulent kinetic energy is just the RANS limit of equation (A3): when ℓ goes to infinity (actually $\ell = L$) all scales are captured, so

$$\langle k \rangle = \frac{3}{2} C \langle \varepsilon \rangle^{2/3} \left(\frac{L}{2\pi} \right)^{2/3} \left[1 - \left(\frac{\eta}{L} \right)^{2/3} \right]. \quad (\text{A4})$$

Using this we can obtain an estimate for f ,

$$f = \left(\frac{\ell}{L}\right)^{2/3} \frac{\left[1 - \left(\frac{\eta}{\ell}\right)^{2/3}\right]}{\left[1 - \left(\frac{\eta}{L}\right)^{2/3}\right]}. \quad (\text{A5})$$

To compute g and R , we need the subfilter enstrophy,

$$\langle \omega'^2 \rangle = \int_{\frac{2\pi}{\ell}}^{\infty} \kappa^2 E(\kappa) d\kappa, \quad (\text{A6})$$

we can use our assumed spectrum to obtain

$$\langle \omega'^2 \rangle = \frac{3}{4} C \langle \varepsilon \rangle^{2/3} \left(\frac{2\pi}{\eta}\right)^{4/3} \left[1 - \left(\frac{\eta}{\ell}\right)^{4/3}\right], \quad (\text{A7})$$

and, therefore,

$$R = 3C_\mu C \frac{\langle \varepsilon \rangle^{2/3}}{\nu^2} \left(\frac{\ell}{2\pi}\right)^{4/3} \left(\frac{\eta}{2\pi}\right)^{4/3} \frac{\left[1 - \left(\frac{\eta}{\ell}\right)^{2/3}\right]^2}{\left[1 - \left(\frac{\eta}{\ell}\right)^{4/3}\right]}. \quad (\text{A8})$$

To find the leading order scaling of R , we can eliminate ε and ν in terms of L and η . To do this, we cannot use the usual dimensional estimates, which are not correct for our stick spectrum. Instead, we must use equation (A4) and

$$\langle \varepsilon \rangle = \nu \langle \omega^2 \rangle = \nu \lim_{\ell \rightarrow \infty} \langle \omega_{<}^2 \rangle = \frac{3}{4} C \nu \langle \varepsilon \rangle^{2/3} \left(\frac{2\pi}{\eta}\right)^{4/3} \left[1 - \left(\frac{\eta}{L}\right)^{4/3}\right]. \quad (\text{A9})$$

With these we find that R scales with Re_t ,

$$R = C_\mu \text{Re}_t \left(\frac{\ell}{L}\right)^{4/3} \frac{\left[1 - \left(\frac{\eta}{L}\right)^{4/3}\right]}{\left[1 - \left(\frac{\eta}{\ell}\right)^{4/3}\right]} \frac{\left[1 - \left(\frac{\eta}{\ell}\right)^{2/3}\right]^2}{\left[1 - \left(\frac{\eta}{L}\right)^{2/3}\right]^2}. \quad (\text{A10})$$

Finally,

$$g = \frac{\langle \mathcal{P}_{<} \rangle}{\langle \varepsilon_{<} \rangle} \approx \frac{\langle \nu_T^{\leq} \rangle \langle \bar{\omega}^2 \rangle}{\nu \langle \omega_{<}^2 \rangle} = R \frac{\langle \bar{\omega}^2 \rangle}{\langle \omega_{<}^2 \rangle}, \quad (\text{A11})$$

or

$$g = \frac{27}{16} C_\mu C^3 \left(1 - \left(\frac{\ell}{L}\right)^{4/3}\right) \left[1 - \left(\frac{\eta}{L}\right)^{4/3}\right]^2 \frac{\left[1 - \left(\frac{\eta}{\ell}\right)^{2/3}\right]^2}{\left[1 - \left(\frac{\eta}{\ell}\right)^{4/3}\right]^2}.$$

If we further consider the case when $\eta \rightarrow 0$, then

$$f = \left(\frac{\ell}{L}\right)^{2/3}$$

$$g = \frac{27}{16}C_\mu C^3 \left(1 - \left(\frac{\ell}{L}\right)^{4/3}\right),$$

or

$$g = \frac{27}{16}C_\mu C^3 (1 - f^2). \quad (\text{A12})$$

References

- [1] Charles G. Speziale and Nessan Mac Giolla Mhuiris. On the prediction of equilibrium states in homogeneous turbulence. *JFM*, 209:591–615, 1989. .
- [2] Sharath S. Girimaji, Eunhwan Jeong, and Ravi Srinivasan. Partially averaged Navier-Stokes method for turbulence: Fixed point analysis and comparison with unsteady partially averaged Navier-Stokes. *J. Appl. Mech.*, 73:422–429, May 2006. .
- [3] Osborne Reynolds. On the dynamical theory of incompressible viscous fluids and the determination of the criterion. *Phil. Trans. Royal Soc. Lond. A*, 186:123–164, 1895.
- [4] G. I. Taylor. Eddy motion in the atmosphere. *Phil. Trans. Royal Soc. Lond. A*, 215:1–26, 1915.
- [5] L. Prandtl. Bericht über untersuchungen zur ausgebildeten turbulenz. *ZAMM - Journal of Applied Mathematics and Mechanics / Zeitschrift für Angewandte Mathematik und Mechanik*, 5(2):136–139, 1925. . URL <https://onlinelibrary.wiley.com/doi/abs/10.1002/zamm.19250050212>.
- [6] J. Smagorinsky. General circulation experiments with the primitive equations: I. The basic experiment. *Mon. Weather Rev.*, 91(3):99–164, March 1963.
- [7] D. K. Lilly. The representation of small-scale turbulence in numerical simulation experiments. In *Proceedings of the IBM Scientific Computing Symposium on Environmental Sciences*, pages 195–210, Yorktown Heights, NY, 1967.
- [8] James W. Deardorff. A numerical study of three-dimensional turbulent channel flow at large Reynolds numbers. *J. Fluid Mech.*, 41, part 2:453–480, 1970. .
- [9] M. Germano. Turbulence: The filtering approach. *J. Fluid Mech.*, 238:325–336, 1992. .
- [10] Stephen B. Pope. *Turbulent Flows*. Cambridge University Press, Cambridge, 2000.
- [11] Stefan H. Johansson, Lars Davidson, and Erik Olsson. Numerical simulation of vortex shedding past triangular cylinders at high Reynolds number using a $k - \varepsilon$ turbulence model. *Inter. J. Numer. Methods Fluids*, 16(10):859–878, 1993. . URL <https://onlinelibrary.wiley.com/doi/abs/10.1002/flid.1650161002>.
- [12] P. A. Durbin. Separated flow computations with the $k - \varepsilon - v^2$ model. *AIAA J.*, 33(4):659–664, 1995. . URL <https://doi.org/10.2514/3.12628>.
- [13] G. Bosch and W. Rodi. Simulation of vortex shedding past a square cylinder with different turbulence models. *Inter. J. Numer. Methods Fluids*, 28(4):601–616, 1998. . URL <https://onlinelibrary.wiley.com/doi/abs/10.1002/%28SICI%291097-0363%2819980930%2928%3A4%3C601%3A%3AAID-FLD732%3E3.O.CO%3B2-F>.
- [14] Andrei Travin, Michael Shur, Michael Strelets, and Philippe Spalart. Detached-eddy simulations past a circular cylinder. *Flow Turb. Comb.*, 63(1):293–313, 2000. . URL <https://doi.org/10.1023/A:1009901401183>.
- [15] G. Iaccarino, A. Ooi, P.A. Durbin, and M. Behnia. Reynolds averaged simulation of unsteady separated flow. *Inter. J. Heat Fluid Flow*, 24(2):147–156, 2003. ISSN 0142-727X. . URL <https://www.sciencedirect.com/science/article/pii/S0142727X02002102>.

- [16] Kyle D. Squires, James R. Forsythe, and Philippe R. Spalart. Detached-eddy simulation of the separated flow over a rounded-corner square. *J. Fluids Eng.*, 127(5):959–966, 09 2005. ISSN 0098-2202. . URL <https://doi.org/10.1115/1.1990202>.
- [17] A. Fadai-Ghotbi, R. Manceau, and J. Borée. Revisiting URANS computations of the backward-facing step flow using second moment closures. Influence of the numerics. *Flow Turb. Comb.*, 81(3):395–414, 2008. . URL <https://doi.org/10.1007/s10494-008-9140-8>.
- [18] E. Palkin, R. Mullyadzhyanov, M. Hadžiabdić, and K. Hanjalić. Scrutinizing URANS in shedding flows: The case of cylinder in cross-flow in the subcritical regime. *Flow Turb. Comb.*, 97(4):1017–1046, 2016. . URL <https://doi.org/10.1007/s10494-016-9772-z>.
- [19] Filipe S. Pereira, Luís Eça, Guilherme Vaz, and Sharath S. Girimaji. On the simulation of the flow around a circular cylinder at $Re = 140,000$. *Inter. J. Heat Fluid Flow*, 76:40–56, 2019. ISSN 0142-727X. . URL <https://www.sciencedirect.com/science/article/pii/S0142727X18306180>.
- [20] P.R Spalart. Strategies for turbulence modelling and simulations. *Inter. J. Heat Fluid Flow*, 21(3):252–263, 2000. ISSN 0142-727X. . URL <https://www.sciencedirect.com/science/article/pii/S0142727X00000072>.
- [21] A. Travin, M. Shur, P. Spalart, and M. Strelets. On URANS solutions with LES-like behaviour. In P. Neittaanmäki, T. Rossi, K. Majava, and O. Pironneau, editors, *Congress on Computational Methods in Applied Sciences and Engineering ECCOMAS*, 2004.
- [22] Sharath S. Girimaji. Partially-averaged Navier-Stokes model for turbulence: A Reynolds-averaged Navier-Stokes to direct numerical simulation bridging method. *J. Appl. Mech.*, pages 413–421, May 2006. .
- [23] Charles G. Speziale. Turbulence modeling for time-dependent RANS and VLES: A review. *AIAA J.*, 36(2):173–184, February 1998.
- [24] Daniel M. Israel, Dieter Postl, and Hermann F. Fasel. A Flow Simulation Methodology for simulation of coherent structures and flow control. AIAA Paper 2004-2225, AIAA, June 2004. 2nd AIAA Flow Control Conference, June 28–July 1, 2004, Portland, OR.
- [25] Hermann F. Fasel, Dominic A. von Terzi, and Richard D. Sandberg. A methodology for simulating compressible turbulent flows. *J. Appl. Mech.*, 73:405–412, MAY 2006. .
- [26] Sharath S. Girimaji and Khaled S. Abdol-Hamid. Partially-averaged Navier Stokes model for turbulence: Implementation and validation. AIAA Paper 2005-502, 2005. 43rd AIAA Aerospace Sciences Meeting & Exhibit, January 10–13, 2005, Reno, NV.
- [27] Bruno Chaouat and Roland Schiestel. A new partially integrated transport model for subgrid-scale stresses and dissipation rate for turbulent developing flows. *Phys. Fluids*, 17(6):065106, 2005. . URL <https://doi.org/10.1063/1.1928607>.
- [28] Roland Schiestel and Anne Dejoan. Towards a new partially integrated transport model for coarse grid and unsteady turbulent flow simulations. *Theor. Comput. Fluid Dynamics*, 18(6):443–468, February 2005. . URL <https://doi.org/10.1007/s00162-004-0155-z>.
- [29] B. E. Launder and D. B. Spalding. The numerical computation of turbulent flows. *Comput. Method Appl. Mech.*, 3:269–289, 1974.
- [30] U. Schumann. Subgrid scale model for finite difference simulations of turbulent flows in plane channels and annuli. *J. Comp. Phys.*, 18(4):376–404, August 1975.
- [31] Akira Yoshizawa. A statistically-derived subgrid model for the large-eddy simulation of turbulence. *Phys. Fluids*, 25(9):1532–1538, September 1982. .
- [32] Mohsen S. Mohamed and John C. Larue. The decay power law in grid-generated turbulence. *J. Fluid Mech.*, 219:195–214, 1990. .
- [33] P. Lavoie, L. Djenidi, and R. A. Antonia. Effects of initial conditions in decaying turbulence generated by passive grids. *J. Fluid Mech.*, 585:395–420, 2007. .
- [34] Sigfried W. Haering, Todd A. Oliver, and Robert D. Moser. Active model split hybrid rans/les. *Phys. Rev. Fld.*, 7:014603, January 2022. . URL <https://link.aps.org/doi/10.1103/PhysRevFluids.7.014603>.
- [35] Colin A. Z. Towery, Juan A. Sáenz, and Daniel Livescu. Posterior comparison of energy partitioning dynamics in several hybrid RANS-LES turbulence models. *In preparation*,

- 2023.
- [36] J. B. Perot and S. M. De Bruyn Kops. Modeling turbulent dissipation at low and moderate Reynolds numbers. *J. Turb.*, 7:N69, 2006. . URL <https://doi.org/10.1080/14685240600907310>.
 - [37] B. E. Morgan and J. A. Greenough. Large-eddy and unsteady RANS simulations of a shock-accelerated heavy gas cylinder. *Shock Waves*, 26(4):355–383, 2016. . URL <https://doi.org/10.1007/s00193-015-0566-3>.
 - [38] Brian M. Haines, Fernando F. Grinstein, and John D. Schwarzkopf. Reynolds-averaged Navier–Stokes initialization and benchmarking in shock-driven turbulent mixing. *J. Turb.*, 14(2):46–70, 2013. . URL <https://doi.org/10.1080/14685248.2013.779380>.
 - [39] J. R. Ristorcelli. Passive scalar mixing: Analytic study of time scale ratio, variance, and mix rate. *Phys. Fluids*, 18(7):075101, Jul 2006. ISSN 1089-7666. . URL <http://dx.doi.org/10.1063/1.2214704>.